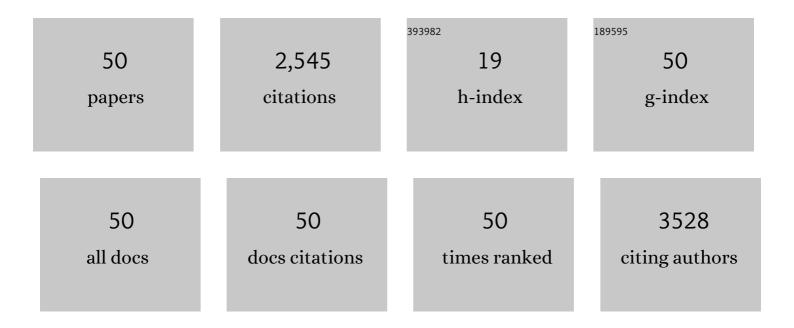
Lan Zhou

List of Publications by Year in descending order

Source: https://exaly.com/author-pdf/5770863/publications.pdf Version: 2024-02-01



#	Article	IF	CITATIONS
1	High Throughput Discovery of Complex Metal Oxide Electrocatalysts for the Oxygen Reduction Reaction. Electrocatalysis, 2022, 13, 1-10.	1.5	7
2	Overcoming Hurdles in Oxygen Evolution Catalyst Discovery via Codesign. Chemistry of Materials, 2022, 34, 899-910.	3.2	17
3	Stability and Activity of Cobalt Antimonate for Oxygen Reduction in Strong Acid. ACS Energy Letters, 2022, 7, 993-1000.	8.8	21
4	Molecular Coatings Improve the Selectivity and Durability of CO ₂ Reduction Chalcogenide Photocathodes. ACS Energy Letters, 2022, 7, 1195-1201.	8.8	6
5	Materials structure–property factorization for identification of synergistic phase interactions in complex solar fuels photoanodes. Npj Computational Materials, 2022, 8, .	3.5	3
6	Addressing solar photochemistry durability with an amorphous nickel antimonate photoanode. Cell Reports Physical Science, 2022, 3, 100959.	2.8	6
7	Band Edge Energy Tuning through Electronic Character Hybridization in Ternary Metal Vanadates. Chemistry of Materials, 2021, 33, 7242-7253.	3.2	7
8	Discovery of complex oxides via automated experiments and data science. Proceedings of the National Academy of Sciences of the United States of America, 2021, 118, .	3.3	21
9	Automating crystal-structure phase mapping by combining deep learning with constraint reasoning. Nature Machine Intelligence, 2021, 3, 812-822.	8.3	29
10	Breaking Scaling Relationships in CO ₂ Reduction on Copper Alloys with Organic Additives. ACS Central Science, 2021, 7, 1756-1762.	5.3	26
11	Quaternary Oxide Photoanode Discovery Improves the Spectral Response and Photovoltage of Copper Vanadates. Matter, 2020, 3, 1614-1630.	5.0	16
12	Enhanced Bulk Transport in Copper Vanadate Photoanodes Identified by Combinatorial Alloying. Matter, 2020, 3, 1601-1613.	5.0	8
13	Bi Alloying into Rare Earth Double Perovskites Enhances Synthesizability and Visible Light Absorption. ACS Combinatorial Science, 2020, 22, 895-901.	3.8	5
14	Combinatorial Synthesis of Oxysulfides in the Lanthanum–Bismuth-Copper System. ACS Combinatorial Science, 2020, 22, 319-326.	3.8	1
15	Successes and Opportunities for Discovery of Metal Oxide Photoanodes for Solar Fuels Generators. ACS Energy Letters, 2020, 5, 1413-1421.	8.8	30
16	Combinatorial screening yields discovery of 29 metal oxide photoanodes for solar fuel generation. Journal of Materials Chemistry A, 2020, 8, 4239-4243.	5.2	13
17	Scanning Electrochemical Flow Cell with Online Mass Spectroscopy for Accelerated Screening of Carbon Dioxide Reduction Electrocatalysts. ACS Combinatorial Science, 2019, 21, 692-704.	3.8	15
18	Investigation of Microstructure and Dispersoids/Precipitates in Additively Manufactured Aluminum Alloys. Microscopy and Microanalysis, 2019, 25, 328-329.	0.2	1

Lan Zhou

#	Article	IF	CITATIONS
19	Multi-modal optimization of bismuth vanadate photoanodes <i>via</i> combinatorial alloying and hydrogen processing. Chemical Communications, 2019, 55, 489-492.	2.2	15
20	Unveiling new stable manganese based photoanode materials <i>via</i> theoretical high-throughput screening and experiments. Chemical Communications, 2019, 55, 13418-13421.	2.2	18
21	The sensitivity of Cu for electrochemical carbon dioxide reduction to hydrocarbons as revealed by high throughput experiments. Journal of Materials Chemistry A, 2019, 7, 26785-26790.	5.2	10
22	Mechanisms of oxide growth during the combustion of Al:Zr nanolaminate foils. Combustion and Flame, 2018, 191, 442-452.	2.8	9
23	Alkaline-stable nickel manganese oxides with ideal band gap for solar fuel photoanodes. Chemical Communications, 2018, 54, 4625-4628.	2.2	2
24	MoS ₂ /TiO ₂ heterostructures as nonmetal plasmonic photocatalysts for highly efficient hydrogen evolution. Energy and Environmental Science, 2018, 11, 106-114.	15.6	326
25	Combinatorial Discovery of Lanthanum–Tantalum Oxynitride Solar Light Absorbers with Dilute Nitrogen for Solar Fuel Applications. ACS Combinatorial Science, 2018, 20, 26-34.	3.8	15
26	Balancing Surface Passivation and Catalysis with Integrated BiVO4/(Fe–Ce)Ox Photoanodes in pH 9 Borate Electrolyte. ACS Applied Energy Materials, 2018, , .	2.5	2
27	Bi-Containing n-FeWO4 Thin Films Provide the Largest Photovoltage and Highest Stability for a Sub-2 eV Band Gap Photoanode. ACS Energy Letters, 2018, 3, 2769-2774.	8.8	20
28	Rutile Alloys in the Mn–Sb–O System Stabilize Mn ³⁺ To Enable Oxygen Evolution in Strong Acid. ACS Catalysis, 2018, 8, 10938-10948.	5.5	97
29	Combinatorial alloying improves bismuth vanadate photoanodes <i>via</i> reduced monoclinic distortion. Energy and Environmental Science, 2018, 11, 2444-2457.	15.6	21
30	Solar fuels photoanode materials discovery by integrating high-throughput theory and experiment. Proceedings of the National Academy of Sciences of the United States of America, 2017, 114, 3040-3043.	3.3	157
31	Automated Phase Mapping with AgileFD and its Application to Light Absorber Discovery in the V–Mn–Nb Oxide System. ACS Combinatorial Science, 2017, 19, 37-46.	3.8	61
32	Electrochemical Stability of Metastable Materials. Chemistry of Materials, 2017, 29, 10159-10167.	3.2	168
33	Discovery of Manganese-Based Solar Fuel Photoanodes via Integration of Electronic Structure Calculations, Pourbaix Stability Modeling, and High-Throughput Experiments. ACS Energy Letters, 2017, 2, 2307-2312.	8.8	36
34	Discovery and Characterization of a Pourbaix-Stable, 1.8 eV Direct Gap Bismuth Manganate Photoanode. Chemistry of Materials, 2017, 29, 10027-10036.	3.2	17
35	X-ray reflectivity measurement of interdiffusion inÂmetallic multilayers during rapid heating. Journal of Synchrotron Radiation, 2017, 24, 796-801.	1.0	15
36	Stability and self-passivation of copper vanadate photoanodes under chemical, electrochemical, and photoelectrochemical operation. Physical Chemistry Chemical Physics, 2016, 18, 9349-9352.	1.3	56

Lan Zhou

#	Article	IF	CITATIONS
37	Solar fuel photoanodes prepared by inkjet printing of copper vanadates. Journal of Materials Chemistry A, 2016, 4, 7483-7494.	5.2	56
38	The role of the CeO ₂ /BiVO ₄ interface in optimized Fe–Ce oxide coatings for solar fuels photoanodes. Journal of Materials Chemistry A, 2016, 4, 14356-14363.	5.2	19
39	High Throughput Light Absorber Discovery, Part 2: Establishing Structure–Band Gap Energy Relationships. ACS Combinatorial Science, 2016, 18, 682-688.	3.8	19
40	Combining reactive sputtering and rapid thermal processing for synthesis and discovery of metal oxynitrides. Journal of Materials Research, 2015, 30, 2928-2933.	1.2	12
41	High Throughput Discovery of Solar Fuels Photoanodes in the CuO–V ₂ O ₅ System. Advanced Energy Materials, 2015, 5, 1500968.	10.2	82
42	Combinatorial thin film composition mapping using three dimensional deposition profiles. Review of Scientific Instruments, 2015, 86, 033904.	0.6	30
43	Room-temperature saturated ferroelectric polarization in BiFeO3 ceramics synthesized by rapid liquid phase sintering. Applied Physics Letters, 2004, 84, 1731-1733.	1.5	992
44	C–V characteristics of Pt/PbZr0.53Ti0.47O3/LaAlO3/Si and Pt/PbZr0.53Ti0.47O3/La0.85Sr0.15CoO3/LaAlO3/Si structures for ferroelectric gate FET memory. Applied Surface Science, 2003, 205, 176-181.	3.1	7
45	Enhanced magnetoresistance of multilayered thin films prepared by pulsed laser deposition. Materials Letters, 2003, 57, 2693-2697.	1.3	1
46	Enhanced dielectric properties of ZrO2thin films prepared in nitrogen ambient by pulsed laser deposition. Journal Physics D: Applied Physics, 2003, 36, 389-393.	1.3	30
47	Photoluminescence of pyrochlore phase in SrBi2Ta2O9 thin films. Applied Physics Letters, 2003, 83, 743-745.	1.5	1
48	Film heterostructure with soft ferromagnetics to enhance low-field magnetoresistance. Applied Physics Letters, 2002, 81, 4073-4075.	1.5	3
49	Properties of SBT films crystallized by pulsed excimer (KrF) laser annealing. Materials Science and Engineering B: Solid-State Materials for Advanced Technology, 2002, 89, 390-393.	1.7	15
50	Defects In 4H Silicon Carbide CVD Epilayers. Materials Research Society Symposia Proceedings, 1996, 442, 631.	0.1	1